Calmodulin inhibitors from the fungus *Emericella* sp.[1]

By: Mario Figueroa, María del Carmen González, Rogelio Rodríguez-Sotres, Alejandro Sosa-Peinado, Martín González- Andrade, Carlos M. Cerda-García-Rojas, Rachel Mata

Figueroa, M., González, M.d.C., Rodríguez-Sotres, R., Sosa-Peinado, A., González-Andrade, M., Cerda-García-Rojas, C.M., Mata, R. (2009). Calmodulin inhibitors from the fungus *Emericella* sp. *Bioorganic and Medicinal Chemistry, 17* (6), pp. 2167-2174. DOI: 10.1016/j.bmc.2008.10.079

Abstract:

Two new xanthones identified as 15-chlorotajixanthone hydrate (**1**) and 14-methoxytajixanthone (**2**) were isolated from an *Emericella* sp. strain 25379 along with shamixanthone (**3**) and tajixanthone hydrate (**4**). The stereostructures of **1** and **2** were elucidated by spectroscopic and molecular modeling methods. The absolute configuration at the stereogenic centers of **1** was established according to CD measurements. In the case of **2**, however, the absolute configuration at C-20 and C-25 was designated as *S* and *R*, respectively, by Mosher ester methodology. Thereafter, the configuration at C-14 and C-15 of **2** was established as *S* and *S*, respectively by comparing the optical rotation and $^{1}H–^{1}H$ coupling constant experimental values with those obtained through molecular modeling calculations at DFT B3LYP/DGDZVP level of theory for diasteroisomers **2a**–**2d**. The activation of the calmodulin-sensitive *c*AMP phosphodiesterase (PDE1) was inhibited in the presence of **1**–**4** in a concentration-dependent manner. The effect of compounds **2** (IC_{50} = 5.54 μM) and **4** (IC_{50} = 5.62 μM) was comparable with that of chlorpromazine (CPZ; IC_{50} = 7.26 μM), a well known CaM inhibitor used as a positive control. The inhibition mechanism of both compounds was competitive with respect to CaM according to a kinetic study. A docking analysis with **2** and **4** using the AutoDock 4.0 program revealed that they interacted with CaM in the same pocket as trifluoropiperazine (TFP).

Graphical abstract

The new xanthones **1** and **2** were isolated from an extract of the mycelium and culture broth of *Emericella* sp. strain 25379 along with two known compounds. The structures of **1** and **2** were elucidated by spectroscopic and molecular modeling methods. The activation of the CaM-sensitive PDE1 was inhibited in the presence of all isolates. A docking analysis revealed that they interacted with CaM in the same pocket of TFP.

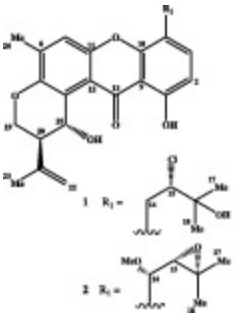

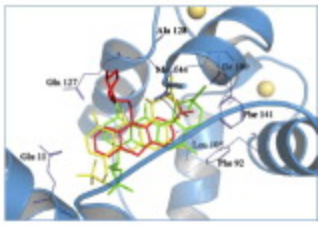

Keywords: *Emericella* | 15-Chlorotajixanthone hydrate | 14-Methoxytajixanthone | Shamixanthone | Tajixanthone hydrate | Calmodulin | Docking

Article:

1. Introduction

The genus *Emericella*, one of the anamorphus of *Aspergillus*,[2] biosynthesizes a remarkable diversity of secondary metabolites with interesting biological properties thus representing potential leads for the developing of new pharmaceutical agents. For example, *E. nidulans* produces antitumor indole alkaloids, prenylated polyketides, benzophenones and xanthones.[3] *E. variecolor* makes simple cytotoxic quinones,[4] indole alkaloids with radical scavenging activity,[5] neuritogenic and antimicrobial polyketides,[6] sesterterpenes,[7] as well as cytotoxic and antimicrobial xanthones.[8, 9] *E. quadrilineata* has yielded some immunostimulant xanthones[10] and tremorgenic alkaloids, while *E. aurantiobrunnea* some variecolin analogues which compete with macrophage inflammatory protein (MIP)-1α for binding to human CCR5 in a scintillation proximity assay.[11] *E. falconensis* and *E. fruticulosa* produce polyketides that inhibit growth of HL60 human leukemia cells and possess antioxidant properties.[12, 13, 14, 15] *E. ungis* generates depsides, depsidones and phthalides.[16] *E. heterothallica*[17, 18] and *E. striata*[19] produce pitetrathiodioxopiperazines which inhibit histamine release and consequently show a remarkable potential as antiallergic agents. *E. violacea* produces biphenyl ether type metabolites[20] and *E. purpurea* indole alkaloids,[21] with *E. rugulosa, E. nidulans, E. astellata* and *E. venezuelensis* the only species that biosynthetize aflatoxins.[22]

Within the scope of a program aiming at the discovery of novel calmodulin (CaM)-inhibitors useful as pesticide or drug leads,[23, 24, 25] herein we report the structure elucidation and CaM-inhibitor properties of two new tajixanthones analogs from a *Emericella* strain isolated from a coral species collected on the Mexican Pacific coast. In addition, to assess their putative binding mode with CaM, a docking analysis was performed. Calmodulin was selected as a molecular target considering its involvement in a variety of cell functions through the regulation of several CaM-dependent enzymes. Modulation of physiological targets of CaM by natural or synthetic compounds offers great possibilities for the discovery of new leads for the development of herbicide or therapeutically useful agents. Indeed certain antipsychotic, smooth muscle relaxants, α-adrenergic blocking, inmunostimulant and cytoprotective drugs, among others, inhibit CaM.[25]

2. Results and discussion

Two new xanthones, namely, 15-chlorotajixanthone hydrate (**1**) and 14-methoxytajixanthone (**2**) were isolated from an *Emericella* sp. strain 25379 along with the known compounds shamixanthone (**3**) and tajixanthone hydrate (**4**).[9] The four natural products were obtained as yellow powders and exhibited UV absorptions at 317, 292, 261 and 249 nm suggesting a hydroxyxanthone chromophore.[9]

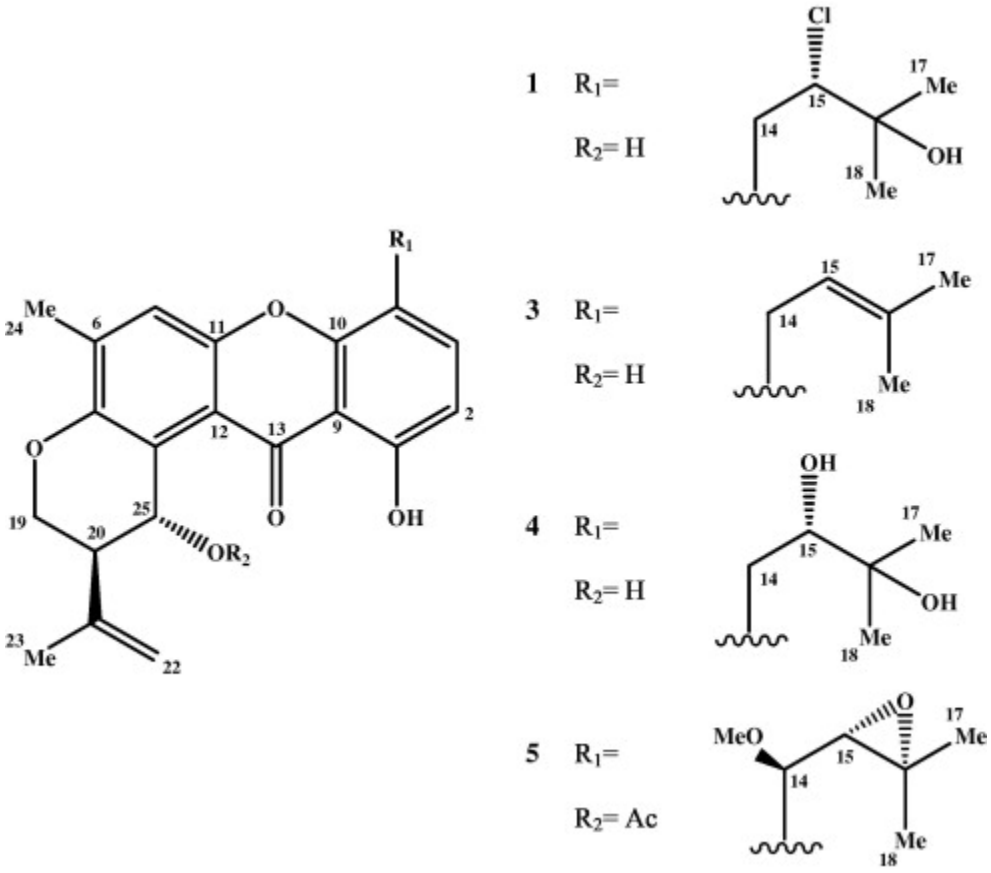

Compound **1** had the molecular formula $C_{25}H_{27}O_6Cl$ which was deduced from the molecular ion in the HREIMS (458.1504, calcd 458.1496). The isotopic pattern in the mass spectrum, with a typical $M/M+2$ ratio of approximately 100:35, revealed the presence of one chlorine atom in the molecule. The ^1H and ^{13}C NMR (Table 1) confirmed the tajixanthone type skeleton[9] and were almost identical to those of compound **4**, differing only in the chemical shifts of the signals of the isoprenyl side chain at C-4. Thus, the spectra of **1** exhibited signals for H-14a, H-14b/C-14 and H-15/C-15 at δ_H/δ_C 3.05, 3.13/28.6 and 3.03/63.4, respectively, rather than δ_H/δ_C 2.63, 3.02/32.0 and 3.70/77.7 suggesting that the hydroxyl group at C-15 in **4** was replaced by a chlorine atom in **1**. The substitution pattern along the xanthone and dihydropyran residues was corroborated by detailed analysis of the HMBC and NOESY spectra (Table 1). Biogenetic considerations, consistent NOESY correlations, and the close correspondence between the Cotton effects of **1** [$\Delta\varepsilon$ (nm) -2.27×10^4 (249), -2.08×10^4 (261), 1.48×10^4 (285), -1.30×10^4 (336)] and those of **4** [($\Delta\varepsilon$ (nm) -1.24×10^5 (245), -8.62×10^4 (260), 3.21×10^4 (292), -4.36×10^4 (336 nm)] strongly supported that the absolute configuration at the stereogenic centers at C-15, C-20 and C-25 was identical in both compounds.

Table 1. NMR data of 15-chlorotajixanthone hydrate (**1**)

Position	Compound 1			
	δ_C	δ_H, mult (*J* in Hz)	HMBC	NOESY
1	160.5		H-2, H-3	
2	137.1	7.53 d (8.0)	H-14a, H-14b	H-14a, H-14b
3	119.3	6.80 d (8.0)	H-2	
4	115.23		H-3, H-14a, H-14b, H-15	
5	109.3	7.33 d (1.0)		H-24
6	138.6		H-24	
7	149.6		H-5, H-19a, H-19b, H-25, H-24	
8	119.3		H-24	
9	109.3		H-2	
10	152.1		H-15, H-14a, H-14b	
11	152.0		H-5	
12	121.1		H-25, H-20	
13	184.4			
14	28.6	a 3.05 brd (16.6) b 3.13 dd (8.0, 16.3)	H-2	H-2, H-17, H-18
15	63.4	3.03 dd (2.0, 10.5)	H-14a, H-14b, H-18, H-17	H-2, H-18
16	116.9		H-14a, H-14b, H-15	
17	24.8	1.34 s	H-18	H-14
18	19.0	1.46 s	H-17	H-15, H-14
19	64.6	a 4.44 ddd (1.0, 3.5, 11.0) b 4.37 dd (3.0, 11.0)	H-25	H-19b, H-20 H-19a, H-20, H-23
20	44.9	2.74 ddd (3.0, 3.0, 3.5)	H-23, H-25, OH-25, H-19a, H-19b, H-22a, H-22b	H-2
21	142.6		H-19a, H-19b, H-25	
22	112.3	a 4.82 ddd (0.5, 1.5, 2.5) b 4.60 dd (1.5, 2.5)	H-23	H-22b, H-25 H-22a, H-23
23	22.5	1.87 t (0.5)	H-22a, H-22b	H-20
24	17.4	2.37 d (1.0)	H-5	
25	63.2	5.43 ddd (1.0, 3.0, 3.5)	OH-25, H-19a, H-19b	H-20, H-23, OH-25, H-22b
OH-1		12.66 d (0.5)		
OH-16		2.47 s		
OH-25		5.03 d (4.0)		

The HRFABMS analysis of **2** gave the molecular formula $C_{26}H_{28}O_7$. The NMR data of **2** (Table 2) indicated that it differed from 14-methoxytajixanthone-25-acetate (**5**) in the presence of a hydroxyl group at C-25 instead of an acetoxy group.[9] Thus compared to **5**, the methine signal for H-25 (δ_H 6.90, s) was diamagnetically shifted to δ_H 5.43 (d, J = 2.1 Hz) in the ^{1}H NMR spectrum of **2**. The position of the substituents in the molecule was also substantiated by careful examination of the HMBC and NOESY spectra (Table 2). The CD spectrum of **2**, however, revealed some significant differences with respect to those of **1** and **4**, which were attributed to the presence of the new chiral center at C-14. In order to establish the absolute configuration at the stereogenic centers in **2**, a combination of molecular modeling calculations and advanced Mosher's methodology was employed.[26] Thus, analysis of the ^{1}H NMR data (Table 2) of the (*S*)- and (*R*)-MTPA esters derivatives **2s** and **2r** prepared from **2**, showed that $\Delta\delta_H$ (*S*–*R*) for H-19a, H-19b and H-20 were +0.0037, +0.0025, and +0.0040, respectively. Therefore, the absolute

configuration at C-20 and C-25 were established as *S* and *R*, respectively; this finding was in agreement with the stereochemistry at these centers for compounds **1**, **3**, **4** and other related xanthones.[9] The configuration at C-14 and C-15 of **2** was next established by comparing the optical rotation and $^{1}H–^{1}H$ coupling constant experimental values with those obtained through molecular modeling calculations[27, 28, 29] at DFT B3LYP/DGDZVP level of theory for diasteroisomers **2a**–**2d**. Figure 1 displays the remarkable differences between the experimental optical rotation of **2** ($[\alpha]_D = –38$) and the calculated[29] values for **2a**, **2c** and **2d**, revealing that the (14*S*,15*S*,20*S*,25*R*)-stereoisomer (**2b**) represents the correct stereochemistry for 14-methoxytajixanthone (**2**). The six more relevant conformers of this substance, including the global minimum **2b**-**1**, are depicted in Figure 2. The free energies, equilibrium populations, coupling constants and $[\alpha]_D$ values for the 28 more populated conformations of **2b** are indicated in Table 3. Moreover, the agreement between the calculated and observed coupling constants $J_{19a,20}$, $J_{19b,20}$ and $J_{20,25}$ confirmed the *trans*-relationship between the substituents at C-20 and C-25 in the dihydropyran ring.

Table 2. NMR data of 14-methoxy-tajixanthone (**2**), (*S*)-MTPA ester of **2** (**2s**), (*R*)-MTPA ester of **2** (**2r**), and $\Delta\delta$ value (δ_{2s}-δ_{2r}) in δ (ppm)

Position	**Compound 2**				**2s**	**2r**	**$\Delta\delta$ value**
	δ_C	**δ_H, mult (*J* in Hz)**	**HMBC**	**NOESY**	**δ_H**	**δ_H**	**($\delta_{2s} - \delta_{2r}$)**
1	162.2		H-2, H-3, OH-1,				
2	135.6	7.72 d (8.5)	H-14a, H-14b, H-15	H-14a, H-14b, H-15			
3	119.0	6.88 d (8.5)	H-2				
4	109.0		H-3, H-14				
5	110.9	7.23 d (1.0)		H-24			
6	138.9		H-24				
7	149.8		H-19a, H-19b, H-24				
8	119.1						
9	116.8		H-3				
10	152.7		H-2				
11	151.9		H-5				
12	115.9						
13	184.4						
14	66.7	3.18 d (8.0)	H-15	H-2, H-17, H-18			
15	76.1	4.67 d (8.0)	H-2, H-14a, H-14b, H-17, H-18, CH_3O-14	H-2, H-18, CH_3O-14			
16	56.9		H-15, H-17, H-18,				
17	24.7	1.25 s	H-18		1.7952	1.7897	+0.0055
18	19.8	1.32 s	H-17	H-15, H-14	1.7523	1.7558	+0.0035
19	64.7	a 4.43 dd (3.6, 10.8)		H-25, H-23	4.4275	4.4238	+0.0037
		b 4.35 dd (3.0, 10.8)			4.3790	4.3765	+0.0025
20	45.0	2.74 ddd (2.1, 3.0, 3.6)	H-19b, H-23, H-22a, H-22b	H-25	2.7350	2.6950	+0.004
21	142.5		H-19b, H-23				
22	112.3	a 4.81 d (2.5)	H-23	H-22b, H-25	4.8060	4.8045	+0.0015
		b 4.60 d (1.0)		H-22a, H-23	4.6160	4.6145	+0.0015
23	22.7	1.85 s	H-22a, H-22b	H-20	1.8391	1.9111	0.072
24	17.5	2.36 s	H-5		2.3490	2.2860	+0.0063
25	63.3	5.43 d (2.1)	H-19a, H-19b	H-20, H-23, H-22b	5.5025	5.4905	+0.012
OH-1		12.86 s					
CH_3O-14	57.8						
OH-25		4.94 brs					

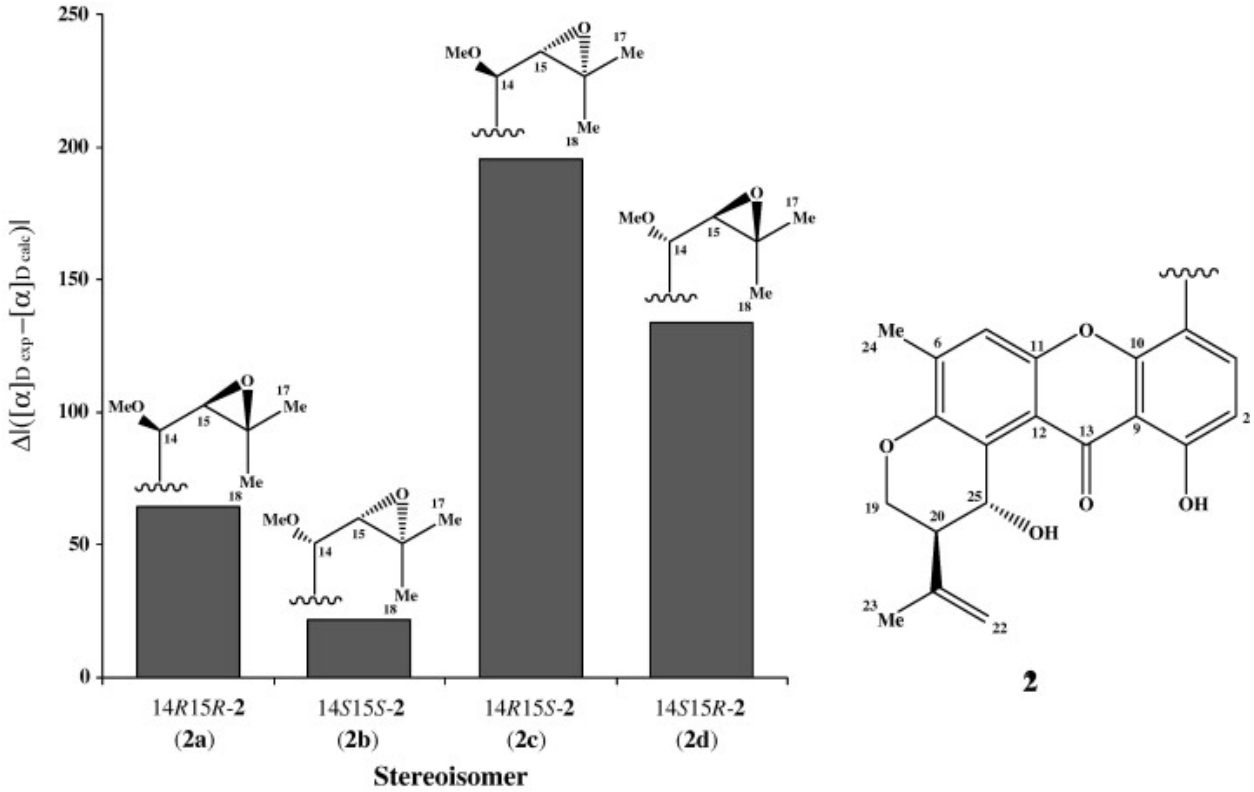

Figure 1. Absolute differences between the experimental optical rotation of 14-methoxytajixanthone (**2**) and the DFT B3LYP/DGDZVP calculated values for stereoisomers **2a**–**2d**. The small difference for (14*S*,15*S*)-**2b** allows the stereochemical assignment of **2**.

The effect of **1**–**4** on CaM was initially assessed with the CaM-sensitive *c*AMP phosphodiesterase (PDE1) assay which is commonly employed to detect CaM antagonists;[23, 25, 30] a human recombinant-CaM was employed as the activator. The results showed that the activation of PDE1 was inhibited in the presence of **2** and **4** in a concentration-dependent manner. The effect of compounds **2** (IC_{50} = 5.54 ± 1.28 μM) and **4** (IC_{50} = 5.62 ± 1.25 μM) was comparable to that of chlorpromazine (CPZ; IC_{50} = 7.26 ± 1.60 μM), a well known CaM inhibitor used as a positive control. A kinetic analysis[31] using different amounts of CaM in the presence of different concentrations of **2** and **4** indicated that both xanthones acted as competitive antagonists of CaM, thus interfering with the formation of the CaM-PDE1 active complex. The estimated K_i (inhibition constant) values were 25.38 ± 2.26 and 13.92 ± 2.29 μM, respectively.

The change of the electrophoretic behavior of CaM treated with the xanthones **1**–**4**, as detected in a PAGE electrophoresis,[32] provided an additional evidence of its interaction with the natural products. According to Figure 3, CaM treated with xanthones **1**–**4** has a lower electrophoretic mobility than the untreated protein. The best effect was observed with compounds **2** and **4**. Upon conducting the same assay in the presence of EGTA, a calcium chelating agent, the mobility of CaM is not retarded indicating that the binding is Ca^{2+}-dependent.

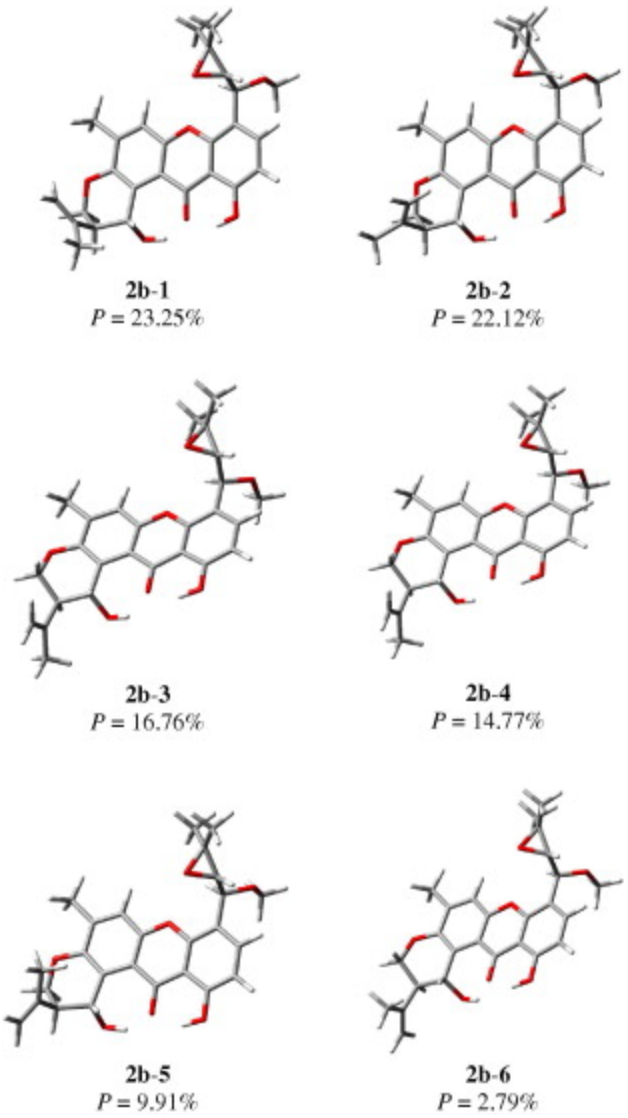

Figure 2. The six more relevant conformations of 14-methoxytajixanthone (**2**) accounting for *ca*. 90% of the conformational population. Substituents at the dihydropyran ring are *pseudo*-axial in structures **2b-1**, **2b-2** and **2b-5** and *pseudo*-equatorial in **2b-3**, **2b-4** and **2b-6**. The conformational arrangement of the isoprene-derived chain remains essentially identical in these structures.

Table 3. Free energies,[a] equilibrium populations,[b] coupling constants,[c] and specific rotation values[d] for conformers 1–28 of (14*S*,15*S*,20*S*,25*R*)-**2**

Conformer	***ΔG***	***P***	$J_{19a,20}$	$J_{19b,20}$	$J_{20,25}$	$J_{14,15}$	$[\alpha]_D$
1	0.00	23.25	1.13	2.98	0.87	9.71	28.34
2	0.03	22.12	1.37	2.44	0.96	9.71	174.63
3	0.19	16.76	11.05	3.39	9.53	9.71	−179.00
4	0.27	14.77	11.05	3.40	9.53	9.71	−176.04
5	0.51	9.91	1.11	3.03	0.77	9.72	28.50
6	1.26	2.79	11.15	3.57	9.03	9.71	−220.72
7	1.47	1.95	1.36	2.46	0.95	9.60	21.38
8	1.71	1.30	1.13	2.98	0.89	9.60	−134.48
9	1.99	0.81	1.13	2.98	0.87	9.53	47.19

Conformer	*ΔG*	*P*	$J_{19a,20}$	$J_{19b,20}$	$J_{20,25}$	$J_{14,15}$	$[\alpha]_D$
10	2.08	0.70	11.07	3.42	9.47	9.58	−307.80
11	2.08	0.70	11.07	3.42	9.46	9.58	−307.77
12	2.08	0.69	1.38	2.44	0.97	9.54	190.90
13	2.09	0.68	1.13	2.97	0.89	1.96	234.91
14	2.28	0.49	1.10	3.05	0.77	9.61	−116.56
15	2.35	0.44	1.36	2.45	0.97	3.59	317.61
16	2.35	0.44	11.05	3.39	9.54	9.56	−165.28
17	2.38	0.42	11.05	3.40	9.54	9.56	−163.95
18	2.51	0.34	1.11	3.04	0.77	9.53	40.98
19	2.57	0.30	1.14	2.96	0.90	3.55	184.51
20	2.57	0.30	1.10	3.07	0.78	1.97	221.75
21	2.63	0.27	1.10	3.06	0.78	3.58	165.93
22	2.94	0.16	11.17	3.60	8.99	9.59	−343.44
23	3.11	0.12	11.15	3.57	9.05	9.55	−204.17
24	3.21	0.10	11.06	3.41	9.50	3.60	−57.10
25	3.55	0.06	1.35	2.48	0.94	9.56	−55.13
26	3.55	0.06	1.13	2.99	0.87	9.57	−212.54
27	3.66	0.05	11.04	3.39	9.49	9.59	−387.57
28	4.08	0.02	1.10	3.06	0.76	9.57	−189.25
Conformational average[e]			4.86	3.01	4.06	9.54	−16.11
Experimental			3.60	3.00	2.75	8.00	−38.00

[a] B3LYP/DGDZVP, in kcal/mol.
[b] Population percentages based on Δ*G*, assuming Boltzman statistics at $T = 298.15$ K and 1 atm.
[c] Coupling constants in Hz calculated from B3LYP/DGDZVP dihedral angles using the Altona equation.
[d] B3LYP/DGZVZP, specific rotation in degrees × [dm × g/cm^3]$^{-1}$.
[e] Σ_i $[\alpha]_D{}^i$, J–$J_{19a,20}{}^i$, J–$J_{19b,20}{}^i$, J–$J_{20,25}{}^i$ or J–$J_{14,15}{}^i \times P^i$, where $[\alpha]_D{}^i$, J–$J_{19a,20}{}^i$, J–$J_{19b,20}{}^i$, J–$J_{20,25}{}^i$, J–$J_{14,15}{}^i$ and P^i are values of $[\alpha]_D$, J–$J_{19a,20}$, J–$J_{19b,20}$, J–$J_{20,25}$, J–$J_{14,15}$ and population in percent for the *i*th conformation.

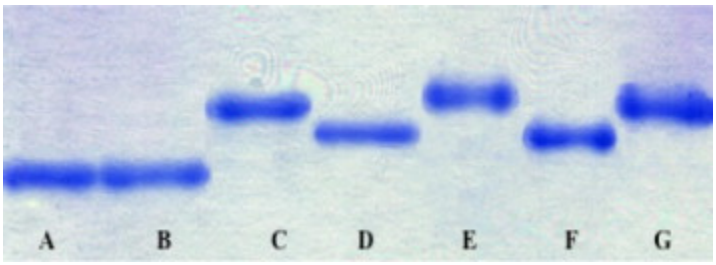

Figure 3. PAGE CaM after treatment with compounds **1**–**4**. Electrophoresis of 2 μg samples of CaM in the presence of 1 mM $CaCl_2$. Pretreatment of the CaM samples, for 1.5 h at 30 °C: (A) no additions; (B) DMSO; (C) 0.033 μg/mL of CPZ; (D) **1**; (E) **2**; (F) **3**; and (G) **4** isolates. In all cases 0.033 μg/mL of **1-4** in DMSO were applied.

To assess the putative binding mode of compounds **1**–**4** with CaM, a docking analysis into the preferred CaM-binding pocket of trifluoropiperazine (TFP) was performed using the advanced docking program AutoDock 4.0.[33] The docking protocol was validated for the CaM crystal structure (pdb code: 1a29) predicting the binding mode of TFP which was removed from the active site and docked back into pocket in the conformation found in its crystal structure.[34] AutoDock successfully predicted the binding mode of TFP with a RMSD (root mean square deviation) of 1.837 Å (Fig. 4). Since CPZ was used as positive control in the assays, the procedure was also validated for this compound (RMSD = 1.931 Å; Fig. 4). The results of molecular docking study revealed that **1**–**4** interacted to the same pocket of TFP and CPZ (Table 4 and Fig. 4). Furthermore, the overall correlation between the K_i and binding affinities predicted

by AutoDock was good, in particular for compounds **2** and **4**. The correlation coefficient (R^2 = 0.971) between the K_i values of **2**, **4** and CPZ and their AutoDock binding free energy values were excellent.

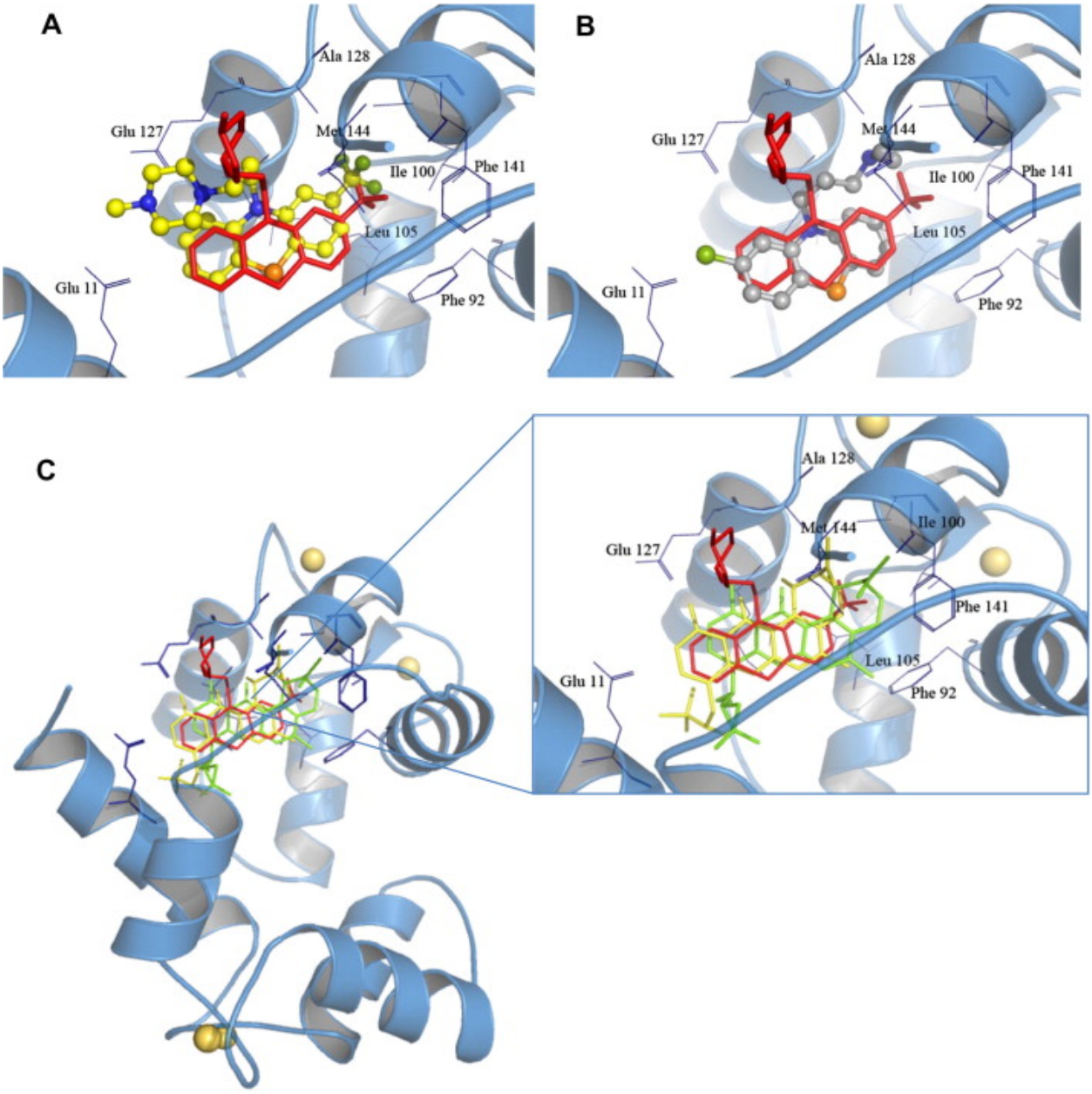

Figure 4. Docking results obtained using AutoDock 4.0 inside the active site of CaM (blue, cartoons). (A) The docked TFP (yellow, ball and stick) and (B) CPZ ligands (grey, ball and stick) into CaM appear superimposed on the cocrystallized TPF (red, sticks). (C) Top ranked binding mode of the most populated cluster of **2** (green, sticks) and **4** (yellow, sticks) into the binding site. Compounds **2** and **4** attach to CaM at the same position than TFP (red, sticks). The metal atoms (Ca^{2+}) are shown as pale-yellow color balls. Hydrogens are omitted for clarity.

Table 4. AutoDock estimated docked energies, binding free energies (ΔGs), calculated and experimental inhibition constants (K_i), and experimental inhibitory concentrations (IC_{50}) of compounds **1**–**4**, CPZ and TFP

Compound	Docked energy (kcal/mol)	*ΔGs* (kcal/mol)	K_i (μM) (calculated)	K_i (μM) (experimental)	IC_{50} (μM)
1	−4.81	−5.14	10.80	ND[a]	9.59 ± 2.65
2	−8.15	−8.38	20.34	25.38 ± 2.26	5.54 ± 1.28
3	−5.11	−5.63	5.77	ND[a]	29.16 ± 6.39
4	−5.08	−4.54	14.36	13.92 ± 2.29	5.62 ± 1.25
CPZ	−6.85	−6.90	8.76	19.28 ± 2.54	7.26 ± 1.60
TFP	−10.06	−10.49	8.36	ND[a]	ND[a]

[a] Not calculated.

In conclusion, the results of the present investigation indicated that *Emericella* sp. contains novel type of competitive CaM-inhibitors. According to AutoDock predictions these compounds interact with the protein at the same binding site of TFP, a well known CaM inhibitor. The CaM antagonist effect of **4** might be related with its mild cytotoxic[9] action and other pharmacological properties yet to be discovered. As with *E. variecolor* and *E. nidulans*, the *Emericella* sp. strain 25379 biosynthesizes tajixhantones type of compounds.

3. Experimental

3.1. General experimental procedures

Optical rotations were obtained on a JASCO DIP 360 digital polarimeter. IR spectra were obtained using KBr disks on a Perkin-Elmer 599B spectrophotometer. The CD spectra of **1**–**4** were obtained on a JASCO 720 spectropolarimeter at 25 °C in $CHCl_3$ solution. UV spectra were recorded on a Shimadzu 160 UV spectrometer in $CHCl_3$ solution. ^1H, ^{13}C and DEPT spectra including 2D NMR were recorded on a Varian Unity Plus 500 or on a Bruker DHX500 in $CDCl_3$ spectrometers at 500 MHz (^1H) or 125 MHz (^{13}C) using tetramethylsilane (TMS) as an internal standard; chemical shifts were recorded as δ values. HREIMS was measured on a JEOL JMS-AX505HA mass spectrometer. Melting point determinations were determined using a Fisher-Johns apparatus and are uncorrected. Preparative HPLC was performed using a Symmetry® C_{18} column [silica gel, 4.6 × 250 mm, 5 μm, 0.6 mL/min]. Control of the equipment, data acquisition, processing, and management of chromatographic were performed by the Empoware® 2 software program (Waters). Open column chromatography: silica gel 60 (0.063–0.200 mm), 70–230 Mesh (Merck).

3.2. Fungal material

Emericella sp. strain 25379 was isolated from the surface of a Coral collected at Marietas Islands in Puerto Vallarta, Jalisco, México, in 2006. Cultures of the fungus are maintained in the mycological collection of the Laboratorio de Micopatología, Instituto de Biología, UNAM. Stock cultures of the fungus were stored at 4 °C on agar plates of potato dextrose agar (PDA). In addition, subcultures were obtained in several culture media, such as PDA, PDA commercial, Czapek Yeast, among others.

3.3. Fermentation and extraction

Ten Fernbach flasks, each containing the liquid medium (2 L/flask) composed of Czapek concentrate (10 mL/L), K_2HPO_4 (1 g/L), powdered yeast extract (5 g/L) and sucrose (30 g/L) were individually inoculated with 1 cm^2 agar plug taken from a stock culture. Flasks were cultures under static conditions at environmental temperature for 30 days. After incubation, the fermented whole broth (20 L) was filtered through cheese cloth to separate into supernatant and mycelia. The former was extracted exhaustively with CH_2Cl_2, and the CH_2Cl_2 solution was concentrated under reduced pressure to give a crude extract (1.5 g). The mycelium was macerated with CH_2Cl_2 (3 × 2 L). The combined organic phase was filtered over anhydrous Na_2SO_4 and concentrated in vacuo to give a dark brown solid (4.0 g).

3.4. Isolation

After evaporating the solvent in vacuo, the combined mycelia and culture (5.0 g) was fractionated by Si gel open CC with a hexane–CH_2Cl_2–EtOAc gradient, to yield 11 primary fractions (F_I–F_{XI}). From fraction F_{IX} (90 mg), eluted with hexane–CH_2Cl_2–EtOAc (4:3.5:2.5), crystallized 18 mg of **4** as a yellow solid. Fraction F_{II} (2 g), eluted with hexane–CH_2Cl_2–EtOAc (7:2:1), was subjected to Si gel CC (45 g) and eluted with a hexane–EtOAc gradient (1:0 → 0:1) to afford four fractions (F_{II-1}–F_{II-4}). Fraction F_{II-2} (70 mg) was further purified by TLC (CH_2Cl_2) to give **3** (15 mg). Fraction F_{IV} (370 mg) was further fractionated on a Sephadex LH-20 (Pharmacia) CC (MeOH) to yield seven secondary fractions (F_{IV-1}–F_{IV-7}). Shephadex fraction F_{IV-7} was resolved on a reverse phase HPLC column, eluting with ACN to yield compounds **1** (8 mg) and **2** (5 mg).

3.4.1. 15-Chlorotajixanthone hydrate (**1**)

Yellow needles, mp 180–181 °C; $[\alpha]_D$ −4.0 (*c* 0.1, $CHCl_3$); IR (KBr) ν_{max} 3486, 3073, 2925, 2849, 1736, 1644, 1567, 1240, 1022, and 920 cm^{-1}; ^1H, ^{13}C, and 2D NMR data, see Table 1; HREIMS $[M]^+$ *m*/*z* 458.1504 (calcd for $C_{25}H_{27}O_6Cl$ 458.1496); CD ($CHCl_3$) (0.057 mg/mL) $\Delta\varepsilon$ (nm) -2.27×10^4 (249), -2.08×10^4 (261), 1.48×10^4 (285), -1.30×10^4 (336); UV λ_{max} ($CHCl_3$) log ε (nm) 3.60 (388), 3.25 (339), 3.76 (301), 3.72 (292), 4.07 (277), 3.96 (258), 3.92 (249), 3.94 (244).

3.4.2. 14-Methoxytajixanthone (**2**)

Yellow needles, mp 200–201 °C; $[\alpha]_D$ −38.0 (*c* 0.1, $CHCl_3$); IR (KBr) ν_{max} 3450, 3078, 2592, 2887, 1795, and 920 cm^{-1}; ^1H, ^{13}C, and 2D NMR data, see Table 2; HRFABMS $[M+1]^+$ *m*/*z* 453.2074 (calcd for $C_{26}H_{28}O_7$ 453.2066); CD ($CHCl_3$) (0.069 mg/mL) $\Delta\varepsilon$ (nm) -5.27×10^4 (247), -2.69×10^4 (260), -2.62×10^2 (295), -9.70×10^3 (301), 1.97×10^2 (317), -1.16×10^4 (335); UV λ_{max} ($CHCl_3$) log ε (nm) 3.23 (395), 2.59 (3.46), 2.48 (299), 3.42 (290), 3.85 (277), 3.74 (261), 3.78 (254), 3.77 (248.5), 3.77 (245).

3.4.3. Shamixanthone (**3**)

Yellow needles, mp 141–143 °C; $[\alpha]_D$ +34.1 (*c* 0.1, $CHCl_3$) [lit. +16.0 (*c* 0.1, $CHCl_3$)]; NMR spectral data were in agreement with those previously described in the literature;[9] CD ($CHCl_3$)

(0.033 mg/mL) $\Delta\varepsilon$ (nm) -2.79×10^4 (263), 2.71×10^4 (295), -1.92×10^4 (336), 1.16×10^4 (446); UV λ_{max} ($CHCl_3$) log ε (nm) 3.50 (395), 2.90 (346), 3.77 (299), 3.76 (293), 4.24 (276), 4.05 (250), 4.07 (244).

3.4.4. Tajixanthone hydrate (**4**)

Yellow needles, mp 182–184 °C; $[\alpha]_D$ −74.0 (*c* 0.1, $CHCl_3$) [lit. −76.0 (*c* 0.23, $CHCl_3$)]; NMR spectral data were in agreement with those previously described in the literature;[9] CD ($CHCl_3$) (0.025 mg/mL) $\Delta\varepsilon$ (nm) -1.24×10^5 (245), -8.62×10^4 (260), 3.21×10^4 (292), -4.36×10^4 (336); UV λ_{max} ($CHCl_3$) log ε (nm) 3.72 (397), 3.14 (347), 3.92 (299), 3.91 (294), 4.42 (278), 4.25 (261), 4.25 (257), 4.21 (249), 4.24 (244).

3.5. Phosphodiesterase activity

The CaM used in this test was recombinant protein over-expressed following *E. coli* BL21-A1™ One shot® vendor procedure (Invitrogen Corp. Carlsbad, CA). Cells BL21-AI were transformed with plasmids pET12-CALM1. Vector construction details will be published elsewhere. Briefly, the expression vector was constructed by amplifying *CALM1* (human phosphorylase kinase, delta) gene by PCR from a cDNA clone pCMV6-XL5, obtained from OriGene (Origene Technology, Inc, Rockville, MD), and subcloned into vector pET12b Novagen (EMD Chemicals Inc., Darmstadt, Germany). After growth for 12 h, cells were harvested by centrifugation and subjected to CaM purification using phenyl-Sepharose CL4B as previously reported.[35, 36, 37] Phosphodiesterase activity was measured according to the method described by Rivero et al.[24] with some modifications. CaM (0.08 μg) was incubated with 0.015 units of PDE1 from bovine brain during 30 min in 40 μL of assay solution containing 0.063 units of 5′-nucleotidase (*Crotalus atrox* venom from Sigma), 45 mM Tris–HCl, 5.6 mM magnesium acetate, 45 mM imidazole, 2.5 mM calcium chloride and 10 μM BSA, pH 7.0. Test compounds were then added to the assay medium at 0.5, 1, 2, 3, 4, 7, 13, 20, 32, 50, and 65 μM in ACN-water (1:1), and the samples incubated during 30 min; thereafter 10 μL of 10.8 mM *c*AMP was added to start the assay. After 15 min, the assay was stopped by the addition of 190 μL of malachite green solution. The amount of inorganic phosphate released, measured spectrophotometrically at 700 nm, correlated with the activity of the PDE1. The experiments to determine K_i values were performed as described above but in the presence of four different concentrations of CaM (25, 50, 100 and 200 ng/mL) and 10 μM BSA. All the results are expressed as the mean of at least six experiments ± SEM. The IC_{50} (concentration inhibiting by 50% the activity of the enzyme) values were determined by non-linear regression analysis by fitting to hyperbolic inhibition (Dixon plot[31]). The K_i was calculated from a global fit of data against inhibitor and CaM concentration using the simple competitive inhibition equation:v=Vm[S]km+BSA1+[I]Ki+[S]Km+BSAwhere V_m = activity at saturating CaM concentration; K_m = dissociation constant of CaM–PDE1 complex; I = concentration of the inhibitor and S = concentration of CaM; BSA = Bovine serum albumine. Non-linear regression was performed with the program Origin 7.0 (OriginLab Corporation, Northampton, MA).

3.6. PAGE of compounds 1–4 with CaM

The interaction of the isolated compounds with CaM was performed using nondenaturing homogeneous electrophoresis (PAGE). PAGE was performed according to previously described procedures using 12% polyacrylamide gels.[32] Interaction of **1**–**4** with CaM was determined by observing the difference in electrophoretic mobility in two different conditions, in the presence of Ca^{2+} and in the presence of EGTA. The experimental conditions are described briefly in the legend of Figure 3. In each case the electrophoresis run was done in triplicate. CPZ was used as the positive control.

3.7. Molecular modeling calculations

A Monte Carlo conformational search[27] for the structures **2a**–**2d** was achieved by molecular mechanics using the MMFF94 force-field as implemented in the Spartan 04 program (Wavefunction Inc. Irvine, CA). In each case, the minimum energy structures were filtered, checked for duplicity and selected within an energy range between 0 and 3 kcal/mol to yield 30, 28, 25, and 22 conformers for **2a**–**2d**, respectively. Each conformer was optimized by DFT at the B3LYP/DGDZVP level of theory[28] using Gaussian W03 (Gaussian Inc., Pittsburg, PA). The fully optimized structures were used to calculate the thermochemical parameters and the frequencies at 298 K and 1 atm. Calculations of the optical rotations[29] were achieved at the same level of theory as well as the ^{1}H–^{1}H vicinal coupling constants. Both properties were Boltzmann-weighted taking into account the DFT conformational population. No solvent effects were included in the calculations.

3.8. Preparation of inhibitor structures

The 3D structures of the studied compounds were constructed using Hyperchem 7.5 (HyperCube Inc., FL). Hydrogen atoms were added to the inhibitor structures. A geometry optimization was performed by applying the PM3 force field in Hyperchem 7.5. For all ligands, random starting positions, random orientations and torsions were used. This allowed searching for flexible conformations of the compounds during the docking process.

3.9. Molecular docking

The docking program AutoDock 4.0 was used to perform the automated molecular docking.[33] The Lamarckian genetic algorithm (LGA) was applied to deal with the inhibitor–enzyme interactions. The grid map with 60 × 60 × 60 points spaced equally at 0.375 Å was generated using the AutoGrid program to evaluate the binding energies between the compounds and the protein. Docking parameters were set to default values except for the number of GA runs (100), the energy evaluations (25,000,000), the maximum number of top individuals that automatically survive (0.1) and the step size for translation (0.2 Å). The docked inhibitor–enzyme complexes were ranked according to the predicted binding energies and to the conformity to ideal geometry of the docked structures.

Acknowledgments

This work was supported by grants of Consejo Nacional de Ciencia y Tecnología (CONACyT, Proyecto 45814-Q). The authors acknowledge Dr. Fabián López-Vallejo for valuable discussion.

The technical assistance of Isabel Rivero-Cruz, Antonio Hernández, Marisela Gutiérrez and Georgina Duarte is also recognized. The authors are very grateful to Dr. A. Olson and his colleagues at the Scripps Research Institute for providing AutoDock. We are indebted to Dirección General de Servicios de Cómputo Académico (DGSCA), UNAM, for providing the resources to carry out computational calculations through KanBalam System. M.F. acknowledges fellowship and the Grant "Apoyo de Tesis Doctoral" from CONACyT.

References and Notes

1. Taken in part from the Ph.D. thesis of M. Figueroa.

2. Samson, R. A.; Hong, S.; Frisvad, J. C. Med. Mycol. 2006, 44, S133.

3. Kralj, A.; Kehraus, S.; Krick, A.; Eguereva, E.; Kelter, G.; Maurer, M.; Wortmann, A.; Fiebig, H.; Koenig, G. M. J. Nat. Prod. 2006, 69, 995.

4. Wang, W.; Zhu, T.; Tao, H.; Lu, Z.; Fang, Y.; Gu, Q.; Zhu, W. J. Antibiot. 2007, 60, 603.

5. Wang, W.; Lu, Z.; Tao, H.; Zhu, T.; Fang, Y.; Gu, Q.; Zhu, W. J. Nat. Prod. 2007, 70, 1558.

6. Wei, H.; Itoh, T.; Kotoku, N.; Kobayashi, M. Heterocycles 2006, 68, 111.

7. Wei, H.; Itoh, T.; Kinoshita, M.; Nakai, Y.; Kurotaki, M.; Kobayashi, M. Tetrahedron 2004, 60, 6015.

8. Malmstrom, J.; Christophersen, C.; Barrero, A. F.; Oltra, J. E.; Justicia, J.; Rosales, A. J. Nat. Prod. 2002, 65, 364.

9. Pornpakakul, S.; Liangsakul, J.; Ngamrojanavanich, N.; Roengsumran, S.; Sihanonth, P.; Piapukiew, J.; Sangvichien, E.; Puthong, S.; Petsom, A. Arch. Pharm. Res. 2006, 29, 140. and references cited therein.

10. Fujimoto, H.; Asai, T.; Kim, Y.; Ishibashi, M. Chem. Pharm. Bull. 2006, 54, 550.

11. Yoganathan, K.; Rossant, C.; Glover, R. P.; Cao, S.; Vittal, J. J.; Ng, S.; Huang, Y.; Buss, A. D.; Butler, M. S. J. Nat. Prod. 2004, 67, 1681.

12. Takahashi, N.; Tamagawa, K.; Kawai, K.; Fukui, T. Biol. Pharm. Bull. 2000, 23, 989.

13. Itabashi, T.; Nozawa, K.; Nakajima, S.; Kawai, K. Chem. Pharm. Bull. 1993, 41, 2040.

14. Itabashi, T.; Nozawa, K.; Miyaji, M.; Udagawa, S.; Nakajima, S.; Kawai, K. Chem. Pharm. Bull. 1992, 40, 3142.

15. (a) Takahashi, N.; Iwahori, A.; Kawai, K.; Fukui, T. Arch. Biochem. Biophys. 1998, 360, 113; (b) Nielsen, J.; Nielsen, P. H.; Frisvad, J. C. Phytochemistry 1998, 50, 263.

16. Kawahara, N.; Nakajima, S.; Satoh, Y.; Yamazaki, M.; Kawai, K. Chem. Pharm. Bull. 1988, 36, 1970.

17. Kawahara, N.; Nozawa, K.; Yamazaki, M.; Nakajima, S.; Kawai, K. Chem. Pharm. Bull. 1990, 38, 73.

18. Kawahara, N.; Nozawa, K.; Nakajima, S.; Yamazaki, M.; Kawai, K. Heterocycles 1989, 29, 397. and references cited therein.

19. Nozawa, K.; Udagawa, S.; Nakajima, S.; Kawai, K. Chem. Pharm. Bull. 1987, 35, 3460.

20. Yamazaki, M.; Maebayashi, Y. Chem. Pharm. Bull. 1982, 30, 509.

21. Hosoe, T.; Itabashi, T.; Kobayashi, N.; Udagawa, S-I.; Kawai, K-I. Chem. Pharm. Bull. 2006, 54, 185.

22. Frisvad, J. C.; Samson, R. A. Syst. Appl. Microbiol. 2004, 27, 672.

23. Mata, R.; Gamboa, A.; Macias, M.; Santillán, S.; Ulloa, M.; González, M. C. J. Agric. Food Chem. 2003, 51, 4559.

24. Rivero-Cruz, B.; Rivero-Cruz, I.; Rodríguez-Sotres, R.; Mata, R. Phytochemistry 2007, 68, 1147.

25. Martínez-Luis, S.; Pérez-Vásquez, A.; Mata, R. Phytochemistry 2007, 68, 1882.

26. Ohtani, I.; Kusumi, T.; Kashman, Y.; Kakisawa, H. J. Am. Chem. Soc. 1991, 113, 4092.

27. Chang, G.; Guida, W. C.; Still, W. C. J. Am. Chem. Soc. 1989, 111, 4379.

28. Godbout, N.; Salahub, D.; Andzelm, J.; Wimmer, E. Can. J. Chem. 1992, 70, 560.

29. Stephens, P.; Pan, J.; Devlin, F.; Cheeseman, J. J. Nat. Prod. 2008, 71, 285.

30. Ovadi, J. In Progress in Drug Research; Jucker, E., Ed.; Birkhauser: Basel, 1989; p 353. Vol. 33.

31. Dixon, M. Biochem. J. 1953, 55, 170–171.

32. Leung, P.; Taylor, W.; Wang, J.; Tripton, C. J. Biol. Chem. 1984, 259, 2742.

33. Morris, G. M.; Goodsell, D. S.; Halliday, R. S.; Huey, R.; Hart, W. E.; Belew, R. K.; Olson, A. J. J. Comp. Chem. 1998, 19, 1639.

34. Paul, M. K.; Mukhopadhyay, A. K. Int. J. Med. Sci. 2004, 1, 101.

35. Hayashi, N.; Matsubara, M.; Takasaki, A.; Titani, K.; Taniguchi, H. Protein Expr. Purif. 1998, 12, 25–28.

36. Persechini, A.; Blumenthal, D. K.; Jarrett, H. W.; Klee, C. B.; Hardy, D. O.; Kretsinger, R. H. J. Biol. Chem. 1989, 264, 8052–8058.

37. Ye, Q.; Li, X.; Wong, A.; Wei, Q.; Jia, Z. Biochemistry 2006, 45, 738.